Exp Fluids (2015) 56:1853
DOI 10.1007/s00348-014-1853-y

RESEARCH ARTICLE

Fast-response temperature-sensitive-paint measurements on a hypersonic transition cone

H. Ozawa · S. J. Laurence · J. Martinez Schramm · A. Wagner · K. Hannemann

Received: 30 May 2014 / Revised: 20 October 2014 / Accepted: 28 October 2014 / Published online: 7 December 2014

Abstract Experiments are performed using a fast-response temperature-sensitive-paint (TSP) technique to measure the heat-flux distribution on a slender cone in a hypersonic shock tunnel under both laminar and transitional conditions. The millisecond-order test duration together with the self-luminosity of shock layers place stringent conditions on the choice of TSP luminophore and the TSP-layer thickness that can be employed. The luminosity and dimming from particulates in the free-stream cause additional problems in interpreting the obtained intensity profiles. Nevertheless, favorable agreement with thermocouple-based measurements show that it is possible to derive quantitatively accurate heat-flux distributions with the TSP technique for temperature rises of up to approximately 40 K above room temperature. The technique accuracy is adversely affected at higher temperatures, which is thought to result from non-constant thermal properties of the insulating base layer. At high unit Reynolds number conditions, time-resolved heat-flux distributions show large-scale unsteadiness in the boundary-layer transition location and reveal transient streamwise streaks developing in the transitional region.

H. Ozawa · S. J. Laurence (✉) · J. M. Schramm · A. Wagner · K. Hannemann
Spacecraft Department, Institute of Aerodynamics and Flow Technology, German Aerospace Center, Bunsenstr. 10, 37073 Göttingen, Germany
e-mail: stuartl@umd.edu

Present Address:
S. J. Laurence
Department of Aerospace Engineering, University of Maryland, College Park, MD 20742, USA

1 Introduction

Vehicles traveling at hypersonic speeds encounter severe heating loads, the accurate quantification of which is crucial for the design of the vehicle's thermal protection system (Bertin and Cummings 2006). Computational fluid dynamics (CFD) studies provide an increasingly powerful tool for the simulation of relevant configurations, but the difficulty in accurately modeling, for example, high-temperature effects, boundary-layer transition and shock-wave/boundary-layer interactions, means that ground-based testing will remain an important tool for evaluating the heating levels encountered by high-speed vehicles for the foreseeable future. Conventional heat-flux sensors, such as thin film gages and thermocouples, have been employed successfully in hypersonic wind tunnels for a number of decades (Schultz and Jones 1973). Such single-point sensors are limited in terms of the spatial resolution they provide; moreover, physical constraints may prevent them being installed in complex geometries. An attractive non-intrusive alternative, providing global heat-transfer measurements at a potentially much lower cost, are temperature-sensitive paints (Liu and Sullivan 2007). A TSP consists of a luminescent molecule (luminophore) mixed with a suitable binder and applied to the surface of the body in question. When illuminated with constant-intensity light at an appropriate wavelength, the intensity of the emitted light is dependent on the surface temperature through a process known as thermal quenching. Thus, through prior calibration, the emission intensity recorded by an imaging device can be related to the temperature at any visualized location on the surface during an experiment. The heat-transfer rate can subsequently be determined from the time sequence of temperature values in a manner outlined shortly.

TSP techniques have been employed in long-duration hypersonic tunnels with varying degrees of ambition (Liu et al. 1995; Kurits and Lewis 2009; Berridge et al. 2010). Their use in short-duration facilities having test times of the order of just a few milliseconds, however, presents a new set of challenges. To provide a sufficiently fast time response, the luminophore employed must have a luminescent lifetime significantly shorter than the test time, excluding otherwise attractive options such as EuTTA dope (~500 μs lifetime). Because the response time scales with the square of the paint thickness, a relatively thin layer (typically $\lesssim$10 μm) is also necessary. In the interests of maximizing the signal intensity at the high frame rates required, however, a thicker layer is desirable; thus, some compromise in layer thickness is unavoidable. The need for high output intensity may further limit the choice of luminophore based on criteria such as quantum efficiency and the availability of a suitable light source. Additional challenges specific to the type of facility employed in the present investigation are discussed later in this article.

The analysis of TSP data in short-duration facilities usually follows that of thin film gages and other conventional sensors for heat-transfer measurement, as described in Schultz and Jones (1973). The TSP coating together with the insulating base layer is treated as a uniform semi-infinite medium, and approximate solutions to the one-dimensional heat-conduction equation with appropriate boundary conditions are sought, allowing the surface heat-transfer rate to be recovered from the time-dependent temperature profile. If the TSP layer is thin enough that it can be assumed to have a negligible effect on the heat-conduction process, the time-varying surface heat-transfer rate, $q_s(t)$, can be obtained using Laplace transforms as:

$$q_s(t) = \sqrt{\frac{\rho_b c_b k_b}{\pi}} \int_0^t \frac{\mathrm{d}T/\mathrm{d}\tau}{\sqrt{t-\tau}} \mathrm{d}\tau, \tag{1}$$

where T is the surface temperature, and ρ_b, c_b, and k_b are the density, specific heat, and thermal conductivity of the base layer. Note that, because of the integral in Eq. (1), we require the entire temperature history to derive the heat flux at a given time. For the special case of a constant heat flux, q_{s0}, the surface temperature assumes a parabolic form:

$$T(t) = 2q_{s0}\sqrt{\frac{t}{\pi \rho_b c_b k_b}}. \tag{2}$$

Equation (2) was used in shock-tunnel measurements by Hubner et al. (2002), who estimated the value of the assumed constant heat flux using a least-squares fit to their derived intensity/temperature data.

If time-resolved heat fluxes are desired from discrete temperature data, the numerical approximation to Eq. (1) proposed by Cook and Felderman (1966) can be used. This approximation assumes only a piecewise linear temperature profile and can be written:

$$q_s(t_n) = 2\sqrt{\frac{\rho_b c_b k_b}{\pi}} \sum_{i=1}^{n} \frac{T(t_i) - T(t_{i-1})}{\sqrt{t_n - t_i} + \sqrt{t_n - t_{i-1}}}. \tag{3}$$

Equation (3) has been used, for example, by Nagai et al. (2008). These authors examined the effect of the TSP-layer thickness on the accuracy of the derived heat flux and concluded that the thickness must be kept smaller than 0.5 μm if Eq. (3) is to be used. The error produced by the finite TSP-layer thickness, however, depends on the relative thermal properties of the base and TSP layers; Nagai et al. (2008) used materials with highly dissimilar properties, and thus, the suggested value of 0.5 μm should not be taken as a fixed rule.

In fact, a relevant analysis of the effect of a finite layer thickness had already been performed by Schultz and Jones (1973) in the context of thin film sensors. The error in the measured heat flux, q_m, was estimated by considering the average temperature over the film thickness in the case of a constant heat flux, q_{s0}. For a TSP-layer/film thickness L, an approximate solution is

$$q_m/q_{s0} = 1 - \frac{L}{\sqrt{\pi \alpha_p t}}\left(\frac{1}{a} - \frac{a}{2}\right), \tag{4}$$

where $\alpha_p = k_p/\rho_p c_p$ and $a = \sqrt{\rho_b c_b k_b/\rho_p c_p k_p}$, the subscript p referring to the TSP-layer/film properties. This solution is valid at large t, i.e., $t \gg L^2/\alpha_p$. The error represented by Eq. (4) effectively has two components: First, differing thermal conductivities of the TSP and base layer will mean that for a given surface temperature rise, the surface heat flux will differ from that which would occur if the TSP layer were absent; and second, because of the nonzero temperature gradient in the TSP layer, the luminescent intensity recorded by the imaging device (corresponding to the average layer temperature) will not be the surface temperature but will always lie somewhere between the temperature at the TSP/insulator interface and the surface temperature. The ratio predicted by Eq. (4) is plotted in Fig. 1 for the TSP- and base-layer properties used in the present experiments and various TSP-layer thicknesses. For timescales typical of mean measurements in shock tunnels as employed in the present investigation (2–4 ms), we see that using a TSP layer of $L = 1.0$ μm would incur a maximum error of ~5 % if no correction for the nonzero thickness were applied.

Methods for dealing with finite TSP-layer thicknesses, however, were proposed by Liu et al. (2010). To address the first error component just referred to, these authors derived a method for recovering the heat flux at the surface of the TSP layer given the time-resolved temperature profile there. The base layer is again assumed to be semi-infinite. The continuous and discretized equations are similar

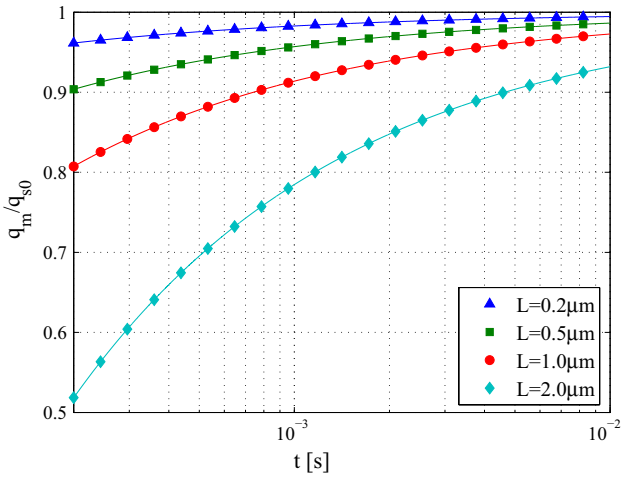

Fig. 1 Ratio of measured heat flux to actual surface heat flux if the influence of the TSP layer is neglected, for various layer thicknesses and using the TSP- and base-layer properties of the present experiments, according to Eq. (4)

Table 1 Typical facility reservoir (subscript 0) and free-stream (subscript ∞) conditions of the three test conditions employed in the present study

	Condition		
	A	B	C
p_0 (Mpa)	12.7	29.3	47.0
h_0 (MJ/kg)	3.3	3.1	3.6
M_∞	7.4	7.4	7.4
Re_∞ (1/m $\times 10^6$)	2.6	6.5	9.8
p_∞ (kPa)	1.44	3.18	5.19
ρ_∞ (g/m^3)	17.9	44.0	67.9
T_∞ (K)	272	251	265
u_∞ (K)	2,420	2,360	2,420
Effective altitude (km)	30.0	24.4	21.4

in form to Eqs. (1) and (3), but with a correction factor in the integral/summation involving a and L. As would be expected, for $L = 0$ or $a = 1$ the original Eqs. (1) and (3) are recovered. An iterative correction for the effective averaging of the temperature over the TSP-layer thickness was also proposed: this is a first-order correction assuming a constant temperature gradient throughout the layer, so cannot be expected to give accurate results for rapidly changing heat fluxes.

As already alluded to, efforts have been made by previous research groups to implement TSP techniques in short-duration hypersonic wind tunnels. Hubner et al. (2002) carried out measurements on a flared double-cone model in two shock tunnels. The original data reduction relied on an assumption of constant heat flux from the onset of the flow, and in situ calibration was found to be necessary, the use of a priori thermal properties resulting in an over-prediction of the heating by 20–50 %. Improved agreement was obtained by Liu et al. (2010) using the methods just described, and then by Cai et al. (2011), the latter employing an algorithm that allowed for temperature-dependent properties of the TSP layer. Japanese researchers have carried out TSP-based heat-flux measurements in the Mach-10 JAXA 0.44-m hypersonic shock tunnel on several geometries including a compression ramp (Ishiguro et al. 2007) and a wing-body model (Nagai et al. 2008). For these experiments, the shock tunnel was run in a mode providing a comparatively long test time (30–50 ms) and low stagnation temperature (~1,200 K). Both these characteristics provide a more forgiving environment for the implementation of TSP techniques; the low stagnation temperature, however, means that the free-stream properties are not representative of flight conditions.

In the present investigation, TSP measurements are performed on a slender transition cone at realistic Mach-8 flight conditions. The short test time of the facility is reduced even further—to the order of a millisecond—by luminosity associated with the high-temperature test gas. Nevertheless, we show it is possible to make quantitatively accurate average heat-flux measurements, and moreover, to gain useful information of a qualitative nature, on such timescales.

2 Test facility and model

2.1 HEG reflected-shock wind tunnel

All experiments were performed in the High Enthalpy Shock Tunnel Göttingen (HEG) of the German Aerospace Center (DLR). HEG is a large-scale reflected-shock wind tunnel, making use of a free piston to generate the driver conditions necessary to reproduce realistic high-speed flows. HEG is capable of simulating a wide range of flow conditions, but like all facilities of its type, is limited in terms of test duration to at most a few milliseconds. It is thus critical that any measurement technique employed has a response time short enough to be able to resolve such timescales. Further information regarding the operating principle of and conditions achievable in HEG is provided, for example, in Hannemann (2003) and Hannemann et al. (2008).

For the present investigation, three test conditions with enthalpies corresponding approximately to Mach-8 flight ($h_0 \approx 3.2$ MJ/kg) and covering a range of Reynolds numbers from 2.6×10^6 to 9.8×10^6 1/m were employed. Representative reservoir and free-stream properties for these three conditions are provided in Table 1. Note that the flow

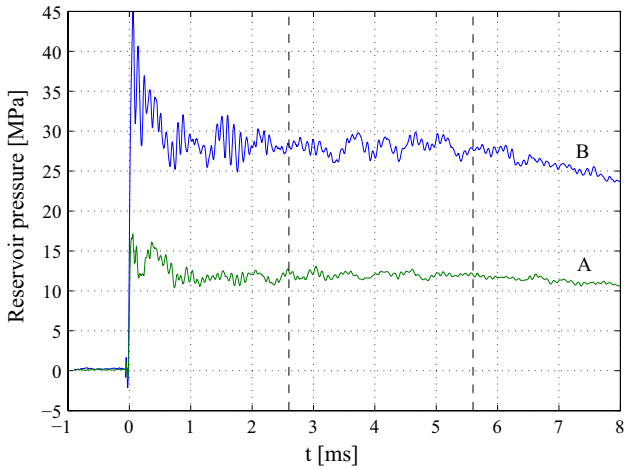

Fig. 2 Typical reservoir pressure traces for two of the three test conditions detailed in Table 1. The approximate test time is indicated by the *vertical dashed lines*

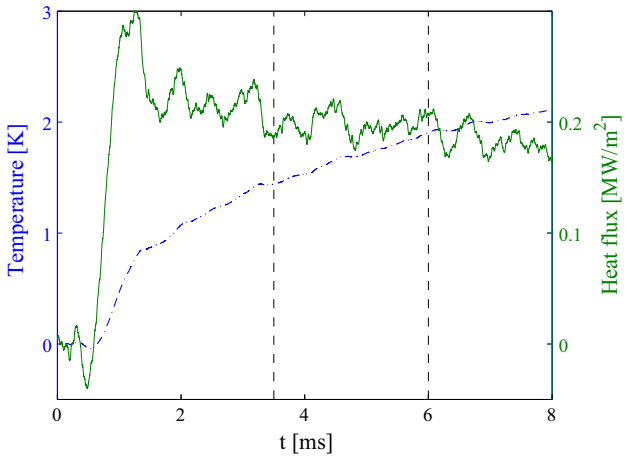

Fig. 3 Typical temperature rise and derived heat-flux profile measured by a thermocouple in HEG (condition B). The approximate test time is indicated by the *vertical dashed lines*

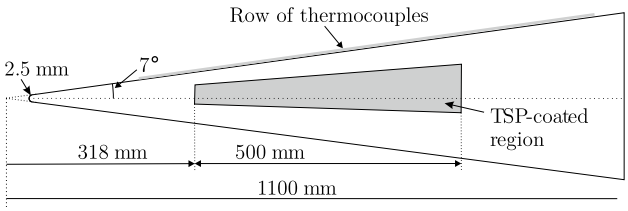

Fig. 4 Schematic of the slender-cone model

was expanded only to Mach 7.4, meaning the static temperature is higher than in flight. The equivalent altitudes were calculated using dynamic pressure matching for Mach-8 flight with standard atmospheric values. Typical reservoir pressure traces for the two conditions from which most of the results will be presented are shown in Fig. 2. These show that, after a start-up period lasting a few milliseconds, steady conditions are attained and persist for approximately 3 ms. Note that there are oscillations in the reservoir pressure even during the nominally steady test time (the standard deviation from the mean in both cases is ∼3.5 %). These oscillations may lead to time variation in the unit Reynolds number and thus unsteadiness in the transition location; this point will be discussed later in the article. The test time is terminated by the arrival of expansion waves in the reservoir, resulting in steadily decreasing pressures thereafter.

Heat-flux measurements in HEG are typically performed with coaxial thermocouples. Figure 3 shows a typical thermocouple temperature trace together with the corresponding heat flux derived using Eq. (3). The latter shows an overshoot during the flow start-up period, before settling to an approximately constant value during the steady test time.

An important consideration for the implementation of TSP and similar techniques in high-temperature wind tunnels such as HEG is the nature of the self-luminosity produced by the facility; the effect of this on TSP measurements is described in more detail in Sect. 3.1. Preliminary spectroscopic measurements have indicated that at conditions in HEG similar to those employed presently, the main broadband background luminosity lies in the longer-wavelength region of the visible spectrum, whereas the emission below ∼500 nm is relatively weak. At higher enthalpies, the main luminosity component shifts to shorter wavelengths.

2.2 Model description

The model employed in the present investigation was a slender 7°half-angle cone that has been used for previous transition research in HEG (Laurence et al. 2012, 2014; Wagner et al. 2013a, b). A schematic of the cone layout is shown in Fig. 4. In all experiments, the model was mounted at nominally zero incidence. The nose radius was 2.5 mm, but for clarity, we will refer to the distance along the cone surface as measured from the extrapolated sharp nose.

The TSP-coated region of the cone was a truncated slice of 500 mm length. First, an approximately 200 μm -thick polyurethane insulating layer was applied to the cone surface; the TSP layer was then painted on this. The insulating layer was sufficiently thick that the semi-infinite approximation referred to in the Introduction was valid over the timescales of interest in HEG. The leading edge of the insulating layer was blended smoothly into the cone body. A row of thermocouples was installed on the ray lying along the top of the cone, approximately 90° offset from the TSP region. In comparing TSP and

thermocouple measurements, we will thus assume that the flow is axisymmetric. For condition A, the cone boundary layer was expected to remain laminar over the coated region, while for conditions B and C, transition was expected toward the middle to front of the coated region.

3 TSP technique

3.1 Challenges associated with applying TSP techniques in HEG

The implementation of luminescent paint techniques in facilities such as HEG is challenging. The demands imposed by the limited test time, common to all short-duration facilities, have been described in the Introduction. Another serious difficulty is posed by the self-luminosity that invariably accompanies the test flow in high-temperature wind tunnels. This luminosity depends strongly on factors such as the stagnation temperature and pressure, the test gas composition, and the model geometry; the combination of relatively low-enthalpy test conditions and a slender model in the present study is comparatively benign in this regard. In TSP measurements, self-luminosity can manifest itself in two ways. First, the luminosity can be directly incident on the imaging device, obscuring or even overwhelming the paint emission. This effect can be mitigated through the use of a narrow band-pass filter and by choosing a luminophore that has a high quantum efficiency and an emission band away from the peak wavelength of the facility luminosity; increasing the intensity of the excitation source as much as possible (subject to any other constraints, such as quenching of the paint) is also desirable for this reason. Second, if the luminosity has a significant component in the absorption band of the luminophore, it can produce additional excitation. This effect is more insidious than the first, since it is more difficult to isolate and cannot be addressed through filtering of the emitted light. In either case, careful selection of luminophore based on knowledge of the spectrum of the facility luminosity at the given test condition is important, as is maximizing the intensity of the excitation source. The latter point can become additionally problematic in large-scale wind tunnels such as HEG, where the test articles (and thus the extent of the region to be be illuminated) are typically larger than in smaller-scale facilities.

A further challenge encountered in the current experiments was the presence of particulate matter in the free stream. This led to a decrease in the detected luminescent intensity, particularly in the flow start-up period prior to the steady test time. Care was taken to clean the facility shock tube before each run, but a certain level of particulate-related dimming was found to be unavoidable in the TSP signal.

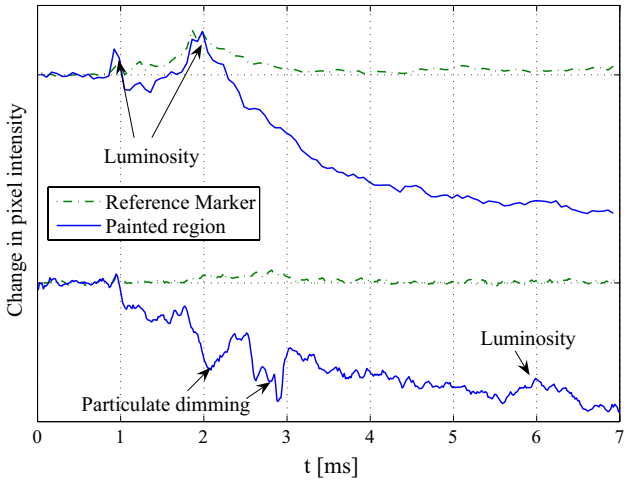

Fig. 5 Changes in pixel intensity recorded on both a TSP-free reference marker and a nearby TSP-coated region for (*above*) a condition-B experiment in which the effects of self-luminosity are dominant and (*below*) a condition-A experiment showing a strong influence of particulate dimming

The effects of luminosity and particulate dimming are illustrated in Fig. 5. In each of the two plotted cases, taken from the experiments described in Sect. 4, we show the time-resolved changes in intensity level recorded on a reference marker (small regions at 100 mm intervals to which no TSP was applied) and on a nearby TSP-coated region. As light at the excitation wavelength is filtered out before reaching the camera, the marker profiles will show increases in intensity only if there is directly incident luminosity, whereas the coated profiles reflect the temperature change with effects of both luminosity and particle dimming superimposed. To isolate all the erroneous effects from the temperature change, small regions of the painted surface could be covered in a transparent, thermally insulating film; this approach has been taken in more recent experiments using a different model. For a "clean" TSP-coated profile, a monotonically and smoothly decreasing intensity reflecting the continuous increase in temperature would be expected (similar to an inverted version of the temperature curve in Fig. 3). The upper curves are taken from a high unit Reynolds number run (condition B) in which the influence of luminosity is dominant over that of particulate dimming. This luminosity is seen most clearly first in the peak at around 1 ms and then in the broader feature reaching a maximum at around 2 ms in both profiles. Thereafter, the marker curve shows the direct luminosity to quickly decrease, though it remains slightly above zero for the remainder of the plotted time. In the lower curves, we make a similar comparison for a low Reynolds number

run (condition A). Here, the marker curve shows only a weak luminosity-related rise between approximately 1.8 and 3.0 ms. In the coated profile, however, strong dips in intensity caused by particulate dimming are observed until 3 ms. Later, from approximately 5.6 ms, an additional spurious peak occurs, apparently caused by luminosity-excited emission (no corresponding direct luminosity is seen in the marker profile). A similar but smaller effect is observed in the upper curve and was in fact seen in all experiments, with an onset time that varied by just a few tenths of a millisecond. In both cases, the earlier luminosity peaks and particulate-related dips have concluded before the beginning of the test time, and a relatively clean measurement period is available before the appearance of the later luminosity peak. Because the derived heat flux is influenced by the entire temperature history, however, the affected parts of the curves before the test time would have to be accounted for.

A simple way to address these early effects is to replace the affected parts of the curves with an assumed profile. In Eq. 1, we see that the integrand has a $\sqrt{t-\tau}$ term in the denominator, meaning that the calculated heat flux at a given time, t, will become less and less influenced by the specified value of the temperature at an earlier time, τ, as t is increased beyond τ. Hence, as long as we make a reasonable estimate of the temperature to replace the initial part of the profile (and also ensure that the chosen measurement time is not too close to the replaced section of the curve), it should be possible to reduce the error in the test-time heat flux to acceptable levels. Considering that there is typically only a limited overshoot in the heat flux prior to the test time (see Fig. 3), Eq. 2 suggests that interpolating with a parabolic profile in the initial part of the temperature curve is a reasonable approximation. For the thermocouple example shown in Fig. 3, if the temperature curve until 3.2 ms is replaced in this way, the error in the calculated heat flux by the beginning of the test time has dropped to 0.1 % and continues to decrease thereafter. If the curve until 3.7 ms is replaced, thus excluding the entire overshoot region, the heat-flux error 0.5 ms later is 2.6 % and has dropped to 0.5 % by the end of the test time at 6.2 ms. Therefore, even in the latter case, the overall mean error will be less than 2 %; given the other uncertainties in the derived heat flux to be discussed shortly, this can be considered an acceptable value.

3.2 TSP selection, calibration and implementation in HEG

A number of considerations, including those mentioned in the previous subsection, were taken into account in selecting the TSP luminophore. A preliminary down-selection was made based on the criterion of a short luminescent lifetime; all candidates were then calibrated for temperature sensitivity and tested to determine the emission and absorption spectra. Ru(phen) (Ruthenium tris(1,10-phenanthroline) dichloride) was chosen as the most promising candidate for its relatively high temperature sensitivity and quantum efficiency, short luminescent lifetime (<1 μs,Mills 1997) and large Stokes shift, and also because its main absorption band is accessible with commercially available blue LED light sources. The measured absorption and emission spectra of Ru(phen) (using a polyacrylic acid (PAA) binder) and the excitation band of the LED source employed are plotted in Fig. 6.

Further experiments were carried out to determine the optimal dye concentration based on emission intensity and temperature sensitivity: The concentration chosen was

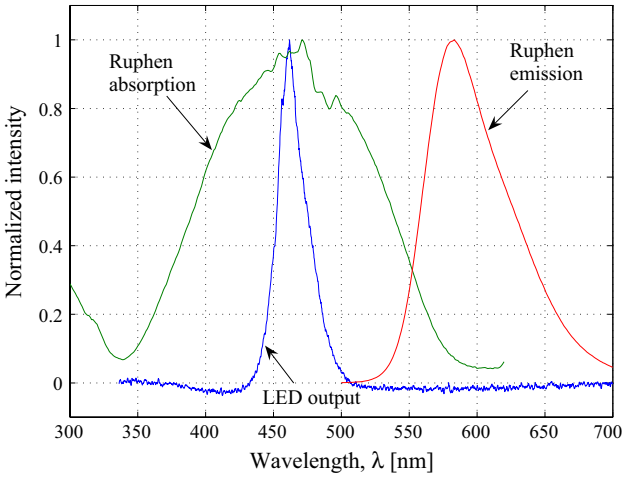

Fig. 6 Measured absorption and emission spectra of Ru(phen), together with the output curve of the blue LED light source

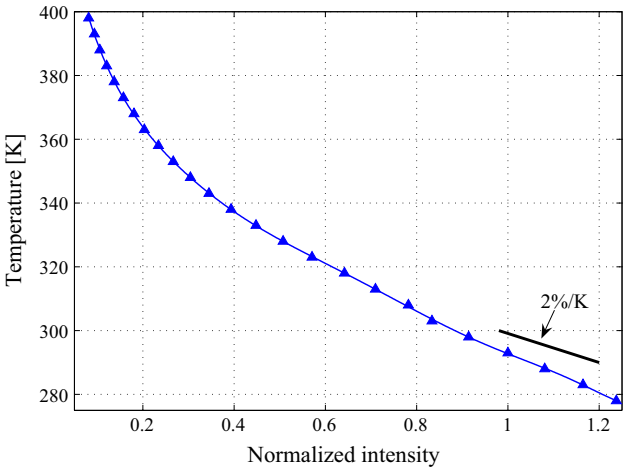

Fig. 7 Measured intensity–temperature calibration curves for Ru(phen) in a PAA binder at 0.16 mol/l together with the fitted polynomial approximation

0.16 mol/l. Experiments were also performed to ensure the pressure sensitivities at the various concentrations were negligible. The intensity–temperature calibration for the chosen concentration is plotted in Fig. 7. The calibration was performed on a 10×10 mm TSP-coated sample in a calibration chamber (LinKam Scientific Instruments TMS94) with the temperature controllable to ± 0.1 K. The temperature was incremented in 5 °C steps from 5 to 125 °C; negligible degradation was observed in return measurements. The pixel-wise variation in the normalized intensity varied from 1 to 2 % (standard deviation) at lower temperatures to approximately 5 % at high temperatures where noise in the imaging device became a major factor. The maximum temperature sensitivity is almost 2.0 %/K close to room temperature, although this drops off significantly above around 350 K. Also shown in Fig. 7 is the 9th-order polynomial curve used in practice to convert intensity into temperature data. The root mean square of the residuals to this fit was 0.21 K; the use of higher-order polynomial fits resulted in a negligible change in the heat flux.

In order to estimate the effect that uncertainty in the calibration would have on the derived heat flux, several repeated coarser calibrations on different samples were performed. Temperatures and heat fluxes from representative intensity curves were then recalculated using the different calibration curves. It was found that the calculated heat-flux values varied by 8–11 % (95 % confidence interval).

For the cone experiments, the TSP-binder mixture was applied with a spray gun to the insulating polyurethane base layer. The hostile flow environment in HEG resulted in degradation in the emitted intensity over several experiments (though with little apparent effect on the sensitivity), meaning the layer had to be re-applied after every 3–4 runs. For runs in between reapplications, the TSP surface was cleaned with a dry cloth. The TSP-layer thickness was coarsely controlled by the number of strokes of the spray gun. Although no direct measurements of the layer thickness were performed, subsequent measurements on a calibrated sample using a profilometer allowed us to estimate the thickness in the HEG experiments based on the volume of liquid applied. The estimated value was $L = 0.2\,\mu$m, although because of the relatively small sample size (and thus higher expected losses), we should consider this the lower bound for the actual tested thickness. The maximum possible thickness based on the TSP-binder volume and application area, assuming zero losses, was approximately 2.5 μm. Later measurements using a larger sample size but a different binder indicated smaller losses that would result in a layer thickness up to 1 μm. Here, we will assume $L = 0.2\,\mu$m but include the possibility of a value up to 1 μm in the uncertainty analysis to follow.

The TSP layer was excited with two LED light sources; images were recorded with a Phantom v641 camera at various frame rates and resolutions. A band-pass filter centered at 600 nm and of width 80 nm was placed in front of the focusing lens of the camera to remove extraneous light. Following each test, the recorded images were analyzed as follows. First, each image was normalized by a reference image created by averaging a number of flow-off images recorded prior to the experiment. The normalized pixel-wise intensity data were then converted into temperatures using the calibration curve shown in Fig. 7. The luminosity- or particulate-affected sections of the temperature curves were removed using the procedure described in Sect. 3.1; finally, heat-flux curves were derived from corrected temperature histories using the method of Liu et al. (2010) referred to in the Introduction. Further details of the heat-flux derivation specific to individual sequences are provided in the following section.

The thermal properties of the base layer at room temperature were measured by an external company using differential scanning calorimetry (specific heat, c_b) and the laser flash method (thermal diffusivity, α_b). The obtained values with uncertainties were $c_b = 1.59\,\text{kJ/kg K} \pm 3\,\%$ and $\alpha_b = 1.09 \times 10^{-7}\,\text{m}^2/\text{s} \pm 7\,\%$. The density was determined as $\rho_b = 1.167 \times 10^3\,\text{kg/m}^3 \pm 10\,\%$. The resulting uncertainty in the heat-flux calculation from these values (see Eq. 1) is thus 11% systematic. Note, however, that these properties were measured only at room temperature: large temperature rises will result in changes in these values (Cai et al. 2011) and thus introduce errors in the derived heat flux. This point will become apparent shortly. The thermal properties of the TSP layer have a much smaller effect on the overall technique accuracy for the thicknesses tested here; values were thus taken from the literature as $\rho_p = 1.41 \times 10^3\,\text{kg/m}^3$, $c_p = 2.76\,\text{kJ/kg K}$, and $k_p = 0.20\,\text{W/m K}$. As noted earlier, there was a relatively high uncertainty in the thickness of the TSP layer: a value of 0.2 μm is assumed but this may realistically be as high as 1 μm. The effect of this uncertainty on the heat flux, however, is limited: As we will demonstrate shortly, a layer of zero assumed thickness versus one of 1 μm produces a difference in the derived heat flux of 4.5% (this could also be concluded from Fig. 1). This will be our assumed value of the uncertainty contribution from the TSP-layer thickness. We will assume a further 1 % contribution from the temperature interpolation described in Sect. 3.1.

Combining the various sources of uncertainty detailed so far (temperature–intensity calibration, thermal properties of base layer, TSP-layer thickness, temperature interpolation), we arrive at an overall experimental uncertainty close to room temperature of 16 % in the derived heat flux. This will be assumed but not plotted in all results shown hereinafter, as it is common to all experiments. In the relevant plots in the following section, error bars will indicate the temporal variation in the derived signals

(which is experiment-specific); this will reflect, for example, image noise and unsteadiness in the free-stream conditions.

4 Experimental results

4.1 Low Reynolds number

First, we describe experiments performed at a low unit Reynolds number (Condition A in Table 1). Since in this case the heat-flux distribution was expected to be one-dimensional, only a narrow visualization window was used (1,280 × 48 pixels); the camera frame rate was set to 63 kfps and the exposure time to 14 µs. Figure 8 presents examples of derived temperature and heat-flux profiles, averaged over a 8 × 2-pixel window. In each plot, we show both the original curve (uncorrected for luminosity or particulate dimming) and the corrected result using an interpolated parabolic temperature profile in the affected section before the test time. The temperature curves have been processed with a 9-point moving-average filter; the heat-flux curves have had an additional 5-point moving-average filter applied. This level of filtering was chosen to be consistent with that typically applied to thermocouple signals in HEG. The chosen test time, shown in dashed vertical lines, is curtailed by the second appearance of luminosity from around 5.5 ms, being thereby restricted to 0.8 ms. Although large oscillations are present early in the uncorrected curves, the resulting change in the average heat flux during the chosen test time is limited to 2% compared to the corrected curve. In this case, the competing effects of luminosity and particulate dimming cancel out one another to a large extent.

In Fig. 9, we show the mean heat-flux distribution over the visualized region. This result is compared to thermocouple measurements as well as a laminar numerical prediction computed using the DLR TAU code (Gerhold et al. 1997) in Fig. 10. In the former, the data has been downsampled to 8 × 2-pixel windows; the latter uses an 8 × 16 -pixel window for each data point. The error bars show the standard deviation arising from the remaining temporal variation following the described smoothing operations. To avoid obscuring the thermocouple data points, error bars for only the first and last TSP points are shown. A decreasing trend in the heat-flux data is clearly visible in both figures, showing that the cone boundary layer remains laminar in the visualized region. The scatter in the TSP data is significantly less than that in the thermocouple measurements, despite the similar magnitude of the error bars. Given the variation in the thermocouple values, the agreement is very good. The TSP curve lies 5–9 % above the simulated CFD profile; although the slope of the upstream portion of the TSP curve (400–450mm) is slightly steeper, downstream

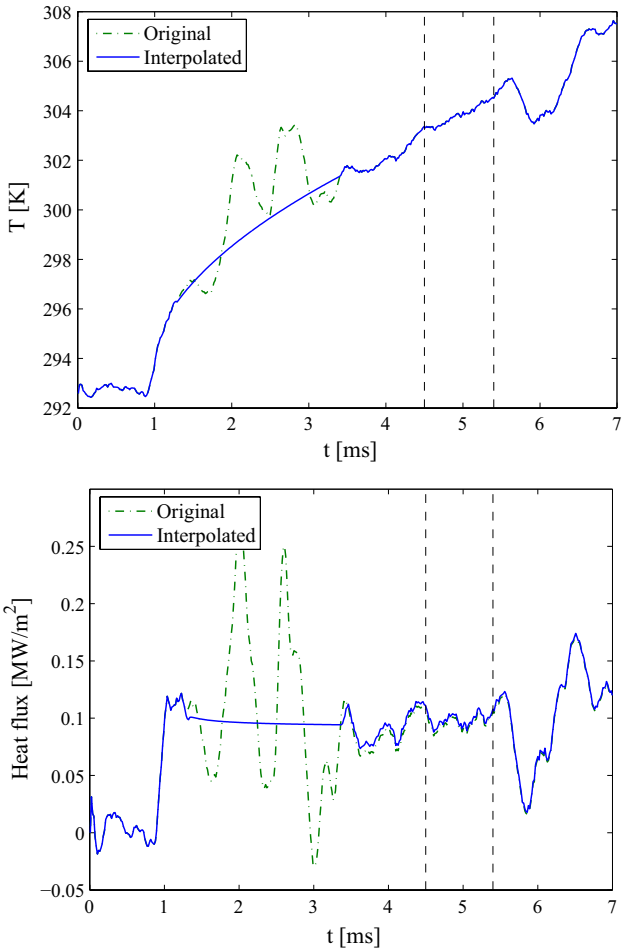

Fig. 8 Time-resolved temperature and heat-flux profiles at a chosen measurement point for a condition-A experiment. The *vertical dashed lines* indicate the chosen test time

the slopes match closely. Considering the experimental uncertainty, this agreement can again be considered very favorable. Also shown is the heat-transfer profile obtained if a TSP-layer thickness of 1.0 µm is assumed in the heat-flux calculation, as referred to earlier. The trend is identical but is shifted upwards by 4 %. A zero-thickness assumption results in the original curve being shifted downward by 0.5 %.

4.2 High Reynolds number

At the higher Reynolds numbers of Conditions B and C, the cone boundary layer was transitional and the heat-flux distribution was expected to become more two-dimensional. For the relevant experiments, the visualization region was thus expanded to gain a more complete picture of the transition process. In Fig. 11, we show an extended heat-flux distribution for a condition-C experiment. In this sequence, the camera was operated with a resolution of 2,048 × 600

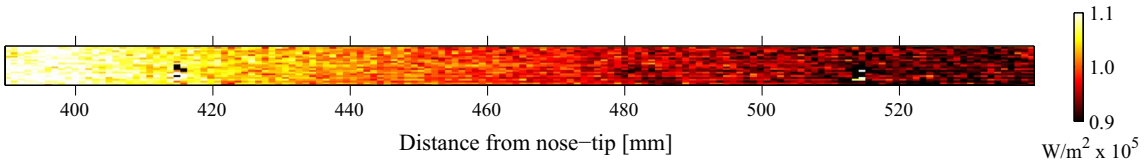

Fig. 9 Heat-flux distribution on the cone surface for a condition-A experiment. The *horizontal* and *vertical scales* are equal in this and all surface-distribution plots hereinafter. Note that the features at 415 and 515 mm are the reference markers

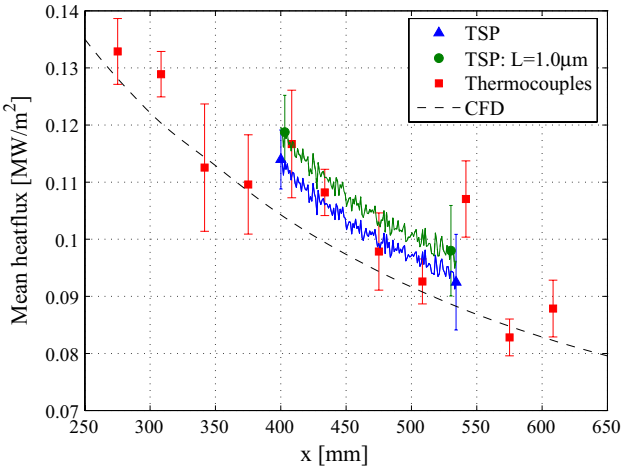

Fig. 10 Comparison of mean heat-flux profiles measured with TSP and thermocouples for the low Reynolds number condition (A), together with that from a numerical simulation of the experiment

pixels, a frame rate of 4.5 kfps, and an exposure time of 50 μs. The reduced frame rate led us to expect that the heat-flux values obtained would be qualitative rather than quantitative, but in fact the agreement with thermocouple measurements was similar to the faster sequences described later in this section. The onset of turbulence in the boundary layer is indicated by a strong streamwise increase in the heat-flux level. The region over which transition develops is seen to be highly two-dimensional, rather than a one-dimensional front. Broad fingers of elevated heating extend into the transitional zone; also notable are narrow, circumferentially intermittent streamwise-aligned streaks in the distribution.

In order to obtain a better understanding of the time-varying nature of the transition process, we now focus on a condition-B experiment in which the images were recorded at a higher frame rate of 16 kfps. The camera resolution and exposure time were 2,560 × 132 pixels, and 61 μs. In Fig. 12, we show temperature and heat-flux profiles obtained in one experiment. Again, we present both original curves and curves making use of interpolated data during the initial luminosity- and particulate-affected period. In this example, it is the effect of luminosity that is dominant, leading to the apparent large dip in temperature that bottoms out at 2 ms. A second luminosity-related dip appears again from 5.5 ms, limiting the effective test time to 1.2 ms. In this case, there is a significant influence of the anomalous signal on the mean heat flux, with the original value exceeding the interpolated value by 13 %.

In Fig. 13 we show the mean heat-flux distribution during the chosen test time. Here, the image has been binned into 8 × 1-pixel windows, and a 3-point temporal

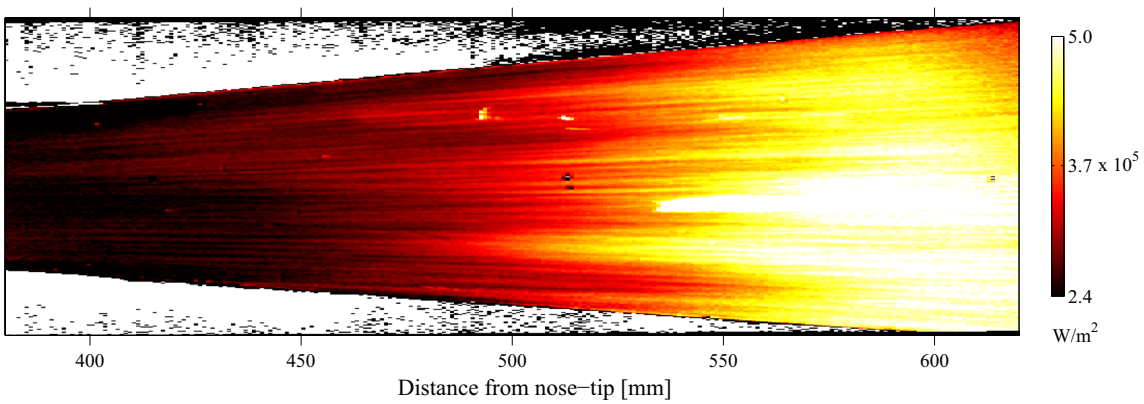

Fig. 11 Mean heat-flux distribution on the cone surface for a condition-C experiment. Note that the bright feature just below the centerline from ~530 mm was caused by a piece of debris striking the cone surface

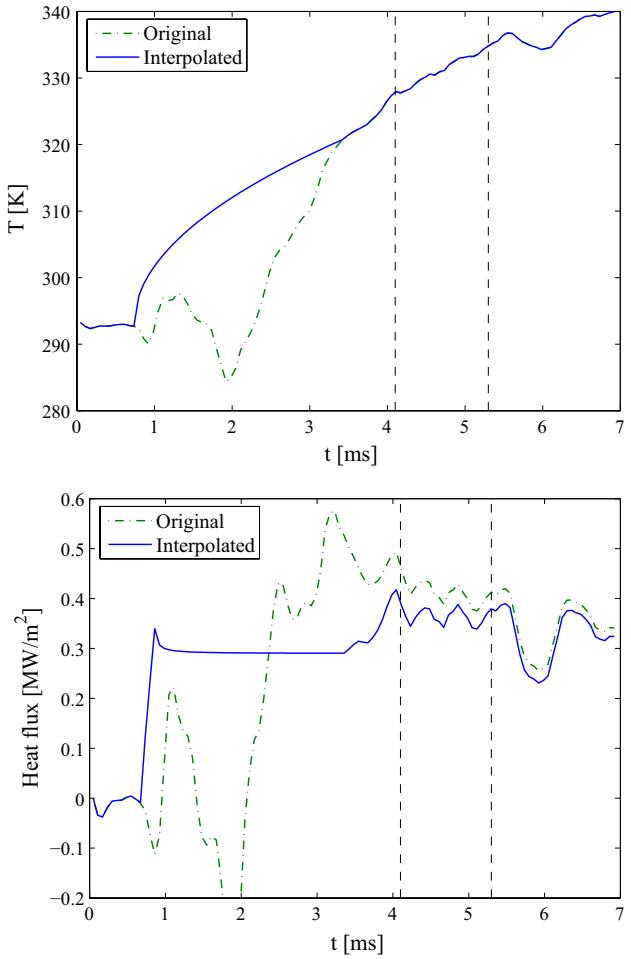

Fig. 12 Time-resolved temperature and heat flux at a measurement point for a condition-B experiment. The *vertical dashed lines* indicate the chosen test time

moving-average filter has been applied to both the temperature and the heat-flux curves. In Fig. 14, we plot heat-flux profiles along the three streamwise rows indicated by white marker lines in Fig. 13 and compare these with the values derived from thermocouple measurements. Error bars indicate the time-varying standard deviation in each case. Both TSP and thermocouples show the expected transitional behavior: a strongly increasing heat flux, reaching a peak value and then beginning to decrease again as the boundary layer becomes fully turbulent. In the early transitional region (470–580 mm), excellent agreement is observed between the TSP and thermocouple results. The TSP curves diverge thereafter, however, and peak at a level approximately 30 % below the maximum thermocouple value.

Results from a repeated experiment at these test conditions are presented in Fig. 15. Here, we show the mean streamwise profile averaged over the lateral width of the window (15.3 mm) and also provide indications of the statistical variation in the lateral direction: mean profiles plus/minus one standard deviation are shown, together with minimum and maximum values at each point in the streamwise direction. The variation is seen to be fairly constant along the curve. Again, we obtain good agreement, with the thermocouples values lying well within the TSP variation, until the heat flux exceeds approximately $3.5 \times 10^5\,\mathrm{W/m^2}$, beyond which even the maximum TSP value begins to underpredict the thermocouple measurements.

This behavior—good agreement for lower values of the heat flux but underprediction of the TSP at higher values (typically above 3–3.5 $\times 10^5\,\mathrm{W/m^2}$)—was consistently observed in several other transitional experiments performed. Considering that the thermocouples and TSP are on different regions of the cone and have different surface properties, it is possible (though unlikely) that this discrepancy is physical. More likely is that, for the high surface temperatures encountered in the later-transitional/turbulent region (constant heat fluxes of 3.5 and $5 \times 10^5\,\mathrm{W/m^2}$ would result in temperature rises after 4 ms of approximately 40 and 60 K, respectively, according to Eq. 2), the thermal properties of the insulating base layer near the surface can no longer be approximated as constant (Cai et al. 2011). While we do not have data on the temperature dependence of the thermal properties of the polyurethane coating used in the present experiments, examples in the literature show that, in particular, the specific heat capacity of polyurethane-based materials can vary strongly with temperature. For instance, Cassel et al. (2012) carried out differential scanning calorimetry measurements on a thermoplastic polyurethane composite and found that the specific heat increased by approximately 50 % from room temperature to 100 °C. Equation 1 shows that such variation would have a direct effect on the measured heat flux. In the future, these variations should be quantified in order to estimate the resulting errors.

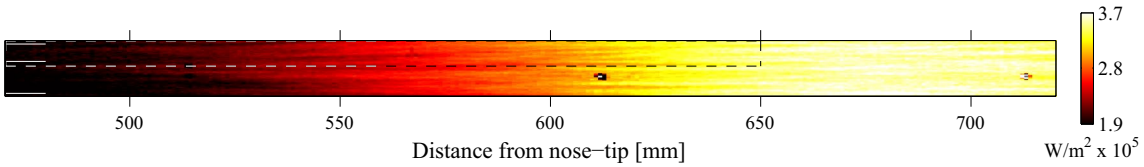

Fig. 13 Mean heat-flux distribution on the cone surface for a condition-B experiment

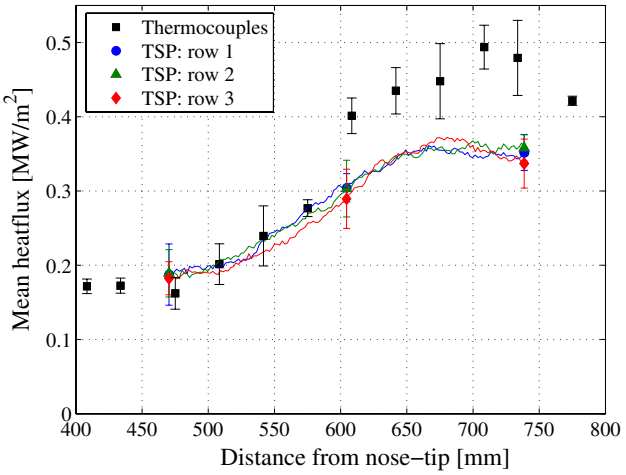

Fig. 14 Mean heat-flux profile for a condition-B experiment derived from thermocouple measurements together with TSP-derived curves at the three locations indicated by markers in Fig. 13 (*row 1* top; *row 3* bottom)

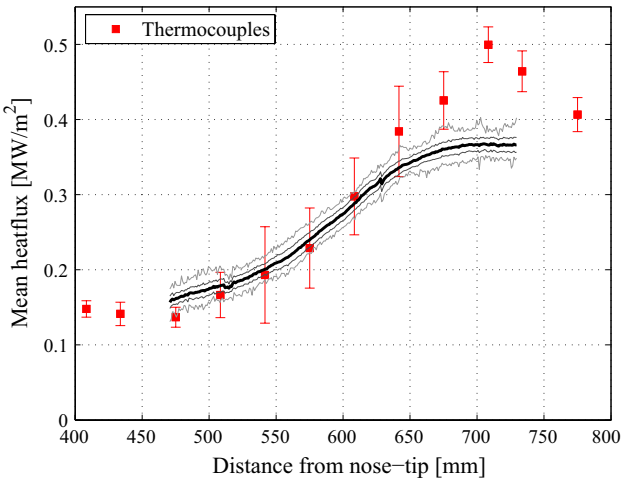

Fig. 15 Mean heat-flux profiles from a second condition-B experiment, showing thermocouple measurements together with the TSP-derived curve averaged in the lateral direction (*thick line*). The inner thin lines show the TSP mean plus and minus one standard deviation, while the outer lines show the minimum and maximum values over the visualized lateral extent

In Fig. 16, we plot heat-flux distributions derived from the same sequence as Fig. 13 but now averaged over consecutive 200 μs time-slices. The location of the transition front is seen to exhibit significant unsteadiness, moving back and forth over a distance on the order of 80 mm during a time period of around 1 ms. For comparison, in Fig. 17, we show a schlieren image sequence of an overlapping region of the cone taken from another condition-B experiment. In the first image, the boundary layer is initially laminar, with transition occurring approximately midway down the window. In subsequent images, the transition location is seen

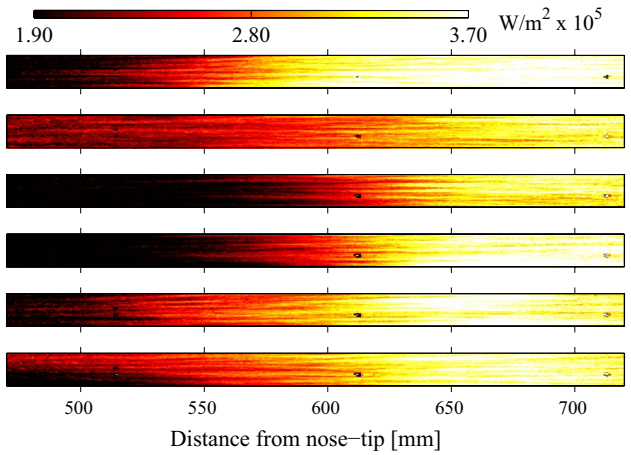

Fig. 16 Time-varying heat-flux distributions taken over consecutive 200 μs increments, calculated from the same data as the averaged distribution shown in Fig. 13

to oscillate substantially in the up- and downstream directions. Such large-scale unsteadiness is probably the cause of the increased standard deviation seen in the thermocouple measurements from around 500 mm in Figs. 14 and 15. We noted in reference to Fig. 2 that there are significant oscillations in the supply pressure which could lead to variations in the free-stream conditions and thus in the transition location during the test time. Assuming the unit Reynolds number to scale linearly through the density with the reservoir pressure, and that the transition Reynolds number remains constant, a ±40 mm variation in transition location at 550 mm would correspond to a ±7 % variation in reservoir pressure, which is twice the standard deviation noted in Fig. 2. Reservoir unsteadiness is thus a reasonable explanation for the shifting of the transition location.

Also prominent in Fig. 16 are the streamwise-aligned streaks referred to earlier. To isolate these from the overall streamwise tendency, in Fig. 18, we present the same 200 μs time-slices (limited to the box enclosed by dashed lines in Fig. 13) with the mean streamwise trend subtracted. These are not truly time-resolved distributions since some degree of temporal smoothing has been applied in deriving the pixel-wise heat-flux profiles; nevertheless, it is clear from these images that the streaks are also highly unsteady in nature, and thus not caused by fixed surface roughness, for example.

In Fig. 19, we plot lateral heat-flux profiles 630 mm downstream of the nose tip for two of the time-slices shown in Fig. 16. The streaks appear here as peaks rising up to 15–20 % above the base heating level. Of particular note in the lower profile, the peaks have a roughly regular spacing of ∼2.5 mm, which is slightly less than twice the laminar boundary-layer thickness computed at this location downstream of 1.4 mm.

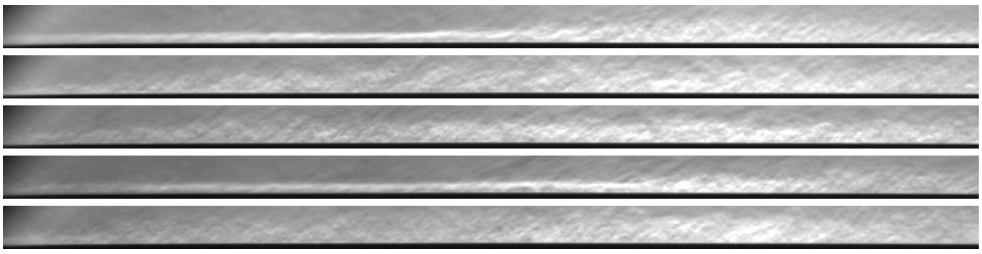

Fig. 17 Schlieren images of the cone boundary layer (590–740 mm from the cone tip) at consecutive 476 μs intervals for a condition-B experiment

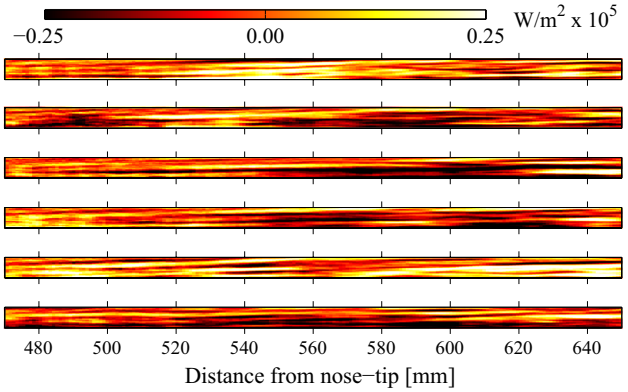

Fig. 18 Heat-flux variation (i.e., with the mean streamwise trend subtracted) within the boxed region shown in Fig. 13, calculated over 200 μs increments

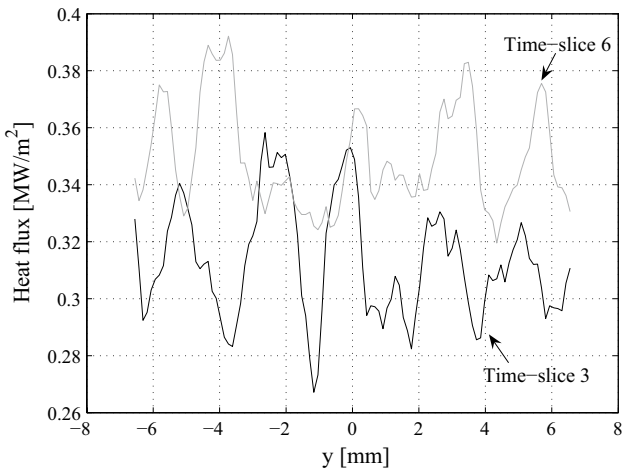

Fig. 19 Heat-flux distribution in the lateral direction, 630 mm from the nose tip, for the third and sixth time-slices shown in Fig. 16

Superficially similar streaks were observed by Berridge et al. (2010) in TSP measurements on a flared cone in quiet Mach-6 flow. In these earlier measurements, however, the streaks must have been caused by steady flow features since the TSP technique employed was incapable of resolving phenomena on short timescales (the camera frame rate was 28 Hz). Under noisy flow the streaks disappeared, or perhaps simply became unsteady. Sivasubramanian and Fasel (2012) performed direct numerical simulations of the breakdown of a second-mode wave packet on a straight cone and, in the case of fundamental breakdown (i.e., that involving a two-dimensional primary wave), obtained streamwise-aligned streaks in heat flux very similar to those observed by Berridge et al. In the case of oblique breakdown, Sivasubramanian and Fasel again saw streamwise streaks, but the circumferential spacing was significantly larger than for fundamental breakdown. In both instances, the streaks were characterized by an initial increase in heating level, a subsequent decrease, and then a second increase to turbulent levels; this was also the case in the experiments of Berridge et al. Such a pattern is not observed here, but it is nonetheless tempting to associate the observed streaks with second-mode breakdown: The measurements in Wagner et al. (2013a) and Laurence et al. (2014) have shown that the second-mode instability is very much active at these conditions; moreover, Kimmel et al. (1996) have shown second-mode wave packets to be limited in their circumferential extent to a few boundary-layer thicknesses or less, which is consistent with the appearance of the streaks in the present experiments. That no decrease in heat flux is observed following the initial rise may be due to the limited ability of the TSP technique to capture the instantaneous heat-flux distribution, i.e., considering the effective temporal resolution and the noisy nature of the flow, even the "time-resolved" distributions plotted here are likely to show the cumulative effect of multiple breakdown events. At this point, we can only speculate about the nature of these streaks; simultaneous high-speed TSP measurements and schlieren images (as in Laurence et al. 2014) may allow us to correlate visualized second-mode wave packets with their surface heat-flux signatures as they saturate and break down, and thus confirm if these streaks really are associated with second-mode breakdown.

5 Conclusions

These experiments have demonstrated the possibility of obtaining global time-resolved heat-flux measurements using a TSP technique in the challenging test environment of HEG. Comparisons with thermocouple-based measurements showed favorable agreement for a total temperature rise of up to ~40 K, though for large temperature changes the technique accuracy was adversely affected, possibly by non-constant thermal properties of the base layer. Measurements at high unit Reynolds number conditions also showed the utility of fast-response TSP techniques for gaining qualitative information, for example, relating to the unsteady boundary-layer transition process.

In these experiments, the effects of tunnel luminosity and particulate dimming were addressed by artificially manipulating the obtained temperature curves; fortuitously, these effects were most severe outside of the steady measurement time. For less benign test conditions, especially higher enthalpy, and model geometries producing stronger shocks (and thus more intense luminosity), such a procedure would probably not be feasible with the present luminophore. Other luminophores, particularly those with excitation and emission peaks lying at shorter wavelengths, may show more promise for such testing. Regardless, the further successful implementation of TSP techniques in facilities such as HEG would benefit greatly from detailed spectral measurements of the tunnel luminosity at the intended test conditions.

Finally, we note that LED technology is advancing rapidly, with light output doubling approximately every 36 months (Nature Photonics Editorial 2007). As increasing the excitation intensity would mitigate many of the problems encountered in the present work, we expect TSP measurements in short-duration facilities to become only more practicable in the future.

Acknowledgments The authors wish to acknowledge the HEG technical staff, in particular Ingo Schwendtke, Mario Jünemann, and Sarah Trost for assistance in preparing the model and running the tunnel. The advice of the DLR Göttingen PSP group, especially Christian Klein, Walter Beck, and Ulrich Henne, was also invaluable during the development and calibration of the TSP technique. We also wish to thank Bryan Schmidt of Caltech and two anonymous reviewers for useful suggestions.

References

Berridge D, Chou A, Ward C, Steen L, Gilbert P, Juliano T, Schneider S, Gronvall J (2010) Hypersonic boundary-layer transition experiments in a Mach-6 quiet tunnel. AIAA paper no. 2010–1061

Bertin J, Cummings R (2006) Critical hypersonic aerothermodynamic phenomena. Annu Rev Fluid Mech 38:129–157

Cai Z, Liu T, Wang B, Rubal J, Sullivan JP (2011) Numerical inverse heat transfer analysis for temperature-sensitive-paint measurements in hypersonic tunnels. J Thermophys Heat Transf 25(1):59–67

Cassel B, Salamon A, Sahle-Demessie E, Zhao A, Gagliardi N (2012) Improved hyperdsc method to determine specific heat capacity of nanocomposites and probe for high-temperature devitrification. Application note, Perkin Elmer

Cook W, Felderman E (1966) Reduction of data from thin-film heat-transfer gages: a concise numerical technique. AIAA J 4(3):561–562

Gerhold T, Friedrich O, Evans J, Galle M (1997) Calculation of complex three-dimensional configurations employing the DLR TAU-code. AIAA paper no. 97–0167

Hannemann K (2003) High enthalpy flows in the HEG shock tunnel: experiment and numerical rebuilding. In: 41st AIAA aerospace sciences meeting and exhibit, Reno

Hannemann K, Martinez Schramm J, Karl S (2008) Recent extensions to the high enthalpy shock tunnel göttingen (HEG). In: Proceedings of the 2nd international ARA days "ten years after ARD", Arcachon

Hubner JP, Carroll BF, Schanze KS (2002) Heat-transfer measurements in hypersonic flow using luminescent coating techniques. J Thermophys Heat Transf 16(4):516–522

Ishiguro Y, Nagai H, Asai K, Nakakita K (2007) Visualization of hypersonic compression corner flows using temperature- and pressure-sensitive paints. AIAA paper no. 2007–118

Kimmel RL, Demetriades A, Donaldson JC (1996) Space-time correlation measurements in a hypersonic transitional boundary layer. AIAA J 34(12):2484–2489

Kurits I, Lewis MJ (2009) Global temperature-sensitive paint system for heat transfer measurements in long-duration hypersonic flows. J Thermophys Heat Transf 23(2):256–266

Laurence SJ, Wagner A, Hannemann K, Wartemann V, Lüdeke H, Tanno H, Itoh K (2012) Time-resolved visualization of instability waves in a hypersonic boundary layer. AIAA J 50(1):243–246

Laurence SJ, Wagner A, Hannemann K (2014) Schlieren-based techniques for investigating instability and transition in a hypersonic boundary layer. Exp Fluids 55:1782

Liu T, Sullivan J (2007) Pressure and temperature sensitive paints. Springer, Berlin

Liu T, Campbell BT, Sullivan JP, Lafferty J, Yanta W (1995) Heat transfer measurement on a waverider at mach 10 using fluorescent paint. J Thermophys Heat Transf 9(4):605–611

Liu T, Cai Z, Lai J, Rubal J, Sullivan JP (2010) Analytical method for determining heat flux from temperature-sensitive-paint measurements in hypersonic tunnels. J Thermophys Heat Transf 24(1):85–94

Mills A (1997) Optical oxygen sensors utilising the luminescence of platinum metal complexes. Platinum Metals Rev 41(3):115–127

Nagai H, Ohmi S, Asai K, Nakakita K (2008) Effect of temperature-sensitive-paint thickness on global heat transfer measurement in hypersonic flow. J Thermophys Heat Transf 22(3):373–381

Nature Photonics Editorial (2007) Haitz's law. Nat Photon 1(23):23

Schultz D, Jones T (1973) Heat-transfer measurements in short-duration hypersonic facilities. AGARDograph no. 165

Sivasubramanian J, Fasel H (2012) Growth and breakdown of a wave packet into a turbulent spot in a cone boundary layer at Mach 6. AIAA paper no. 2012–85

Wagner A, Hannemann K, Kuhn M (2013a) Experimental investigation of hypersonic boundary-layer stabilization on a cone by means of ultrasonically absorptive carbon-carbon material. Exp Fluids 54:1–10

Wagner A, Hannemann K, Wartemann V, Giese T (2013b) Hypersonic boundary-layer stabilization by means of ultrasonically absorptive carbon–carbon material, part 1: experimental results. AIAA paper no. 2013–270